Vol 17 No 5, May 2008
1674-1056/2008/17(05)/1769-08

Chinese Physics B

© 2008 Chin. Phys. Soc.
and IOP Publishing Ltd

Study on holographic grating diffraction for Laguerre–Gaussian beam generation*

Liu Yi-Dong(刘义东)†, Gao Chun-Qing(高春清)‡, and Gao Ming-Wei(高明伟)

Department of Optical-Electronics, School of Science and Technology, Beijing Institute of Technology, Beijing 100081, *China*

(Received 20 July 2007; revised manuscript received 27 September 2007)

Laguerre–Gaussian beams, as a special model with spiral phase structure, have been intensively investigated. Holographic grating method is a convenient method of generating Laguerre–Gaussian beams and measuring their orbital angular momenta. But due to some inevitable adverse factors such as lateral displacement, angular deflection and elliptical incident profile of incident beam, the practical effectiveness should be reevaluated. This paper is devoted to the study on the influences of the abovementioned three adverse factors on the holographic grating method. The characteristics of the mode decomposition of diffractive order and the relative powers of the orbital angular momentum eigen-states are also given.

Keywords: Laguerre–Gaussian beam, orbital angular momentum, holographic grating
PACC: 4225B, 4230K, 4260H

1. Introduction

Orbital angular momentum is a novel physical parameter of a beam, and it has attracted much attention recently. Allen *et al*[1] have experimentally found that a beam with a phase structure $\exp(il\varphi)$ has an orbital angular momentum with a quantity $l\hbar$ and an the azimuthal number l. The Laguerre–Gaussian beam and the Bessel beam are two particular examples of such beams. Since Allen *et al*'s work,[1] the applications of beams with orbital angular momenta have been in full flourish in many areas, such as optical tweezers and optical spanners,[2−6] astronomy application,[7] quantum information application (data storage,[8,9] high density data transformation,[10] quantum data processing[11,12]) and orbital angular momentum imaging.[13]

The generation of Laguerre–Gaussian beams is important for studying the orbital angular momenta of beams. Many methods have been used to achieve such a goal, such as inner cavity mode selection method,[14] and mode convertor consisting of cylindrical lenses,[15,16] spiral phase plate,[17,18] and holographic grating.[19−21] The measuring of orbital angular momenta of beams is also an essential topic in studying the beams with orbital angular momenta, and the interferometric sorter[22,23] and the holographic grating[19,20] have been developed to fulfil such a task. The holographic grating is a more convenient method either of generating the Laguerre–Gaussian beams or of measuring their orbital angular momenta because it is easy to design by using computer and able to realize complex patterns.[19,20] The orbital angular momentum spectrum dispersion is influenced by many factors, such as the misaligned optical system.[24] In our recent work we have studied the influences of the misaligned optical system and elliptical incident beam on the generation of the Laguerre–Gaussian modes experimentally.[25]

The present paper is devoted to discussing the generation of Laguerre–Gaussian beams by using amplitude gratings. The influences of the incident beam with lateral displacement, angular deflection and elliptical profile are further discussed. The theoretical analyses show the effects of these factors on the orbital angular momentum spectrum and mode decomposition, which gives us a new visual angle to understand these effects.

*Project supported by the Doctorate Fund of the State Education Commission of China (Grant No 20050007027), the National Natural Science Foundation of China (Grant No 60778002) and the Program for New Century Excellent Talents in University (NCET), China.

†E-mail: liu_yd@bit.edu.cn
‡Corresponding author. E-mail: gao@bit.edu.cn

2. Generation of Laguerre–Gaussian beam and detection of orbital angular momentum

As is well known, a Laguerre–Gaussian beam has eigen-solution of the slowly varying envelope approximation wave equation in cylindrical coordinates. When a Laguerre–Gaussian beam propagating along the z-axis interferes with a unitary planar beam propagating along the direction (sinθ, 0, cosθ) which deflects from the z-axis by an angle θ, the phase structure reads

$$\Phi(\rho,\varphi,z) = l\varphi - \frac{k\rho^2}{2R} - (2p+l+1)\,\Psi + kx\sin\theta + kz(\cos\theta - 1), \tag{1}$$

where $R(z)$ is the curvature radius of the wave-front of Laguerre–Gaussian beam, $\Psi(z)$ the Gouy phase, l the azimuthal number, p the radial number, and $k = \omega/c$ the wave number. Consider that at $z = 0$, i.e. at the waist of Laguerre–Gaussian beam, the curvature radius $R = 0$ and Gouy phase $\Psi = 0$, then the phase structure will reduce to a simple form as follows:

$$\Phi(\rho,\varphi,0) = l\varphi + kx\sin\theta. \tag{2}$$

A grating with such a structure is a fork-like grating with l dislocations in the centre when the planar beam is oblique-axial with respect to the Laguerre–Gaussian beam or a helical grating with l fringes twisted together when it is coaxial with the Laguerre–Gaussian beam.

An amplitude grating in the pattern determined by the wave structure in expression (2) reads

$$T(\rho,\varphi) = a(\Phi(\rho,\varphi,0)), \tag{3}$$

where $a(*)$ denotes the amplitude structure, e.g. the binary amplitude grating takes the form

$$a(\Phi) = \begin{cases} 1.0, & \mod(\Phi, 2\pi) \le \pi, \\ 0.0, & \text{otherwise.} \end{cases} \tag{4}$$

This amplitude structure function can be expanded into Fourier series as follows:

$$a(\Phi) = \sum_{n=-\infty}^{+\infty} A_n \exp(in\Phi). \tag{5}$$

For the binary amplitude grating, the expansion coefficients read

$$A_n = \frac{\sin(n\pi/2)}{n\pi}\exp\left(-\frac{in\pi}{2}\right). \tag{6}$$

For other kinds of structures, e.g. the sinusoidal grating or blazing grating, and phase grating or amplitude grating, a similar operation of expression (5) also holds. For simplicity, the binary amplitude grating is used here. Figure 1(a) gives the phase structure determined by expression (2) with one dislocation in the centre. Figure 1(b) gives the binary amplitude constructed from the phase structure in Fig.1(a) by using expression (4).

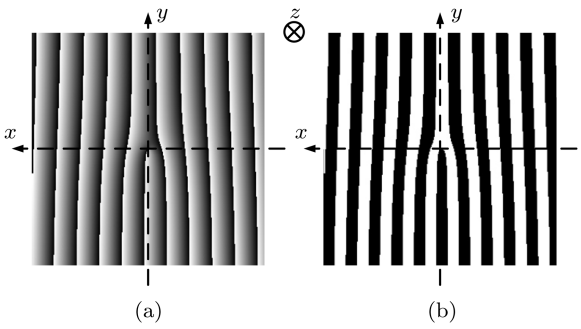


Fig.1. (a) Phase structure of fork grating with one dislocation in the centre, where the dark regions are for 0 and the white regions are for 2π. (b) Binary amplitude grating with structure determined in (a).

When illuminated by the Laguerre–Gaussian beam $u_{00}^{\mathrm{LG}}(\rho,\varphi)$ with a radial number (p) of 0 and an azimuthal number (l) of 0, the diffractive field behind the grating is

$$u_{\mathrm{i}}(\rho,\varphi) = u_{00}^{\mathrm{LG}}(\rho,\varphi)\cdot T(\rho,\varphi). \tag{7}$$

The from of the far-field diffractive beam can be considered to be the Fourier transform of u_{i}, and it is denoted as

$$u_{\mathrm{f}}(\rho',\varphi') = F[u_{\mathrm{i}}(\rho,\varphi)], \tag{8}$$

where F denotes the two-dimensional Fourier transform and superscripts depict the variances in spatial-frequency domain, and (ρ', φ') are the polar coordinates in spatial-frequency domain. A usual method of deriving the analytical expression of $u_{\mathrm{f}}(\rho', \varphi')$ is to decompose it as a superposition of Laguerre–Gaussian beams and apply the two-dimensional Fourier transform of Laguerre–Gaussian beam.[26]

$$F[u_{p,l}(\rho,\varphi)] = \mathrm{i}^{2p+|l|}2\pi u_{p,l}^{\mathrm{LG}}(\rho',\varphi'). \tag{9}$$

After derivation we can obtain the far field distribution as follows:

$$u_{\mathrm{f}}(\rho',\varphi') = 2\pi\sum_{n=-\infty}^{+\infty} A_n\cdot\sum_{p=0}^{+\infty} c_p\mathrm{i}^{2p+|nl|}u_{p,nl}^{\mathrm{LG}}(\rho',\varphi') \otimes[\delta(\omega_x - nk\sin\theta)\,\delta(\omega_y)], \tag{10}$$

where $\otimes$ denotes the convolution; $(\omega_x,\ \omega_y)$ is the Cartesian presentation coordinates related to the polar coordinates presentation $(\rho',\ \varphi')$ by $\omega_x = \rho'\cos\varphi$ and $\omega_y = \rho'\sin\varphi$; c_p is the decomposition coefficient of the diffractive field in expression (7) behind the Laguerre–Gaussian beams and expressed as

$$c_p = \int_0^{+\infty}\int_0^{2\pi} u_{00}^{\mathrm{LG}}(\rho,\varphi) \cdot \exp(\mathrm{i}nl\varphi)\cdot u_{p,nl}^{\mathrm{LG}^*}(\rho,\varphi)\,\rho\mathrm{d}\rho\mathrm{d}\varphi. \quad (11)$$

From expression (10), the far field diffractive pattern can be considered to be the superposition of Laguerre–Gaussian beams with the nth diffractive beam that has a side shifted by $nk\sin\theta$ and an azimuthal quantum number changed by nl, but with different radial numbers in the spatial frequency domain. A similar analysis holds for the case of high order Laguerre–Gaussian mode illumination.

3. Generation of Laguerre–Gaussian beam in general case

In practical applications we often find the beam transformation in a perfect condition. In this paper the effects of the lateral displacement, angular deflection and elliptical profile will be discussed. Figure 2 shows the three kinds in a nonideal case that will be discussed below.

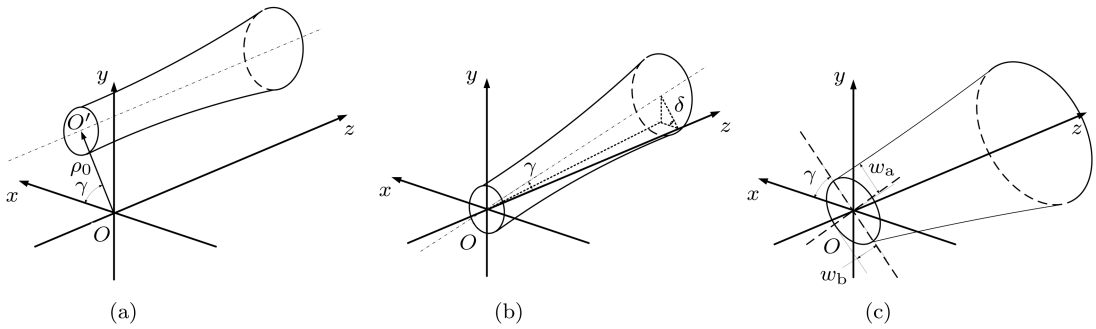


Fig.2. Three kinds of non-ideal cases. (a) Lateral displacement, (b) Angular deflection, and (c) Elliptical-profile.

3.1. Lateral displacement of incident beams

Now we discuss that the incident beam has a lateral displacement relative to the optical system as shown in Fig.2(a). Dot line denotes the axis of the incident beam, which is parallel to the axis of the optical system. The incident beam shifts from the z-axis radially and azimuthally by ρ_0 and γ, respectively.

Assuming that the incident beam is a shifted fundamental Laguerre–Gaussian beam $u_{00}^{\mathrm{LG}}(\rho,\varphi)$ and it can be written in polar coordinates as

$$u'(\rho,\varphi) = u_{00}^{\mathrm{LG}}(\rho,\varphi)\exp\left(-\frac{\rho_0^2}{w_0^2}\right) \times \exp\left[\frac{2\rho\rho_0\cos(\varphi-\gamma)}{w_0^2}\right]. \quad (12)$$

For a further study, we expand expression (12) into a superposition of spiral harmonics (or the superposition of Laguerre–Gaussian beams). As shown in expression (9), the two-dimensional Fourier transformation has a simple form. Then the beam in expression (12) can be rewritten as

$$u'(\rho,\varphi) = u_{00}^{\mathrm{LG}}(\rho,\varphi)\exp\left(-\frac{\rho_0^2}{w_0^2}\right)\sum_{m=-\infty}^{+\infty} I_m\left(\frac{2\rho\rho_0}{w_0^2}\right) \times \exp[\mathrm{i}m(\varphi-\gamma)], \quad (13)$$

where I_m is an mth order modified Bessel function.[27] In this way we expand the shifted fundamental Laguerre–Gaussian beam into the superposition of spiral harmonics $\exp(\mathrm{i}m\varphi)$.[28]

Replacing $u_{00}^{\mathrm{LG}}(\rho,\varphi)$ in expression (7) by the shifted beam as shown in expression (13) and following a similar procedure in expression (8), we can obtain the far field distribution as follows:

$$u_{\mathrm{f}}(\rho',\varphi') = 2\pi\sum_{n=-\infty}^{+\infty} A_n \sum_{m=-\infty}^{+\infty}\exp(-\mathrm{i}m\gamma) \times \sum_{p=0}^{+\infty} c_{pm}\mathrm{i}^{2p+|m+nl|}u_{p,m+nl}^{\mathrm{LG}}(\rho',\varphi') \otimes[\delta(\omega_x - nk\sin\theta)\,\delta(\omega_y)], \quad (14)$$

where

$$c_{pm} = \int_0^{+\infty}\int_0^{2\pi} u_{00}^{\mathrm{LG}}(\rho,\varphi)\exp\left(-\frac{\rho_0^2}{w_0^2}\right) I_m\left(\frac{2\rho\rho_0}{w_0^2}\right) \times \exp\left(\mathrm{i}\left(m+nl\right)\varphi\right) u_{p,m+nl}^{\mathrm{LG}^*}(\rho,\varphi)\,\rho\mathrm{d}\rho\mathrm{d}\varphi. \tag{15}$$

3.2. Angular deflection of incident beams

The second kind of factor is the angular deflection of the incident beam with a deflection angle η and an azimuth γ, as shown in Fig.2(b). Then the axial wave number can be written as

$$k_z = \sqrt{k^2 - k_\rho^2} \approx k - k_\rho^2/2k. \tag{16}$$

We can represent a deflected beam as the beam passing through a phase wedge with the transmission function $\exp[\mathrm{i}\alpha\rho\cos(\varphi-\delta)]$ where $\alpha = k_\rho = k\ \sin\gamma$.[24] Then the incident fundamental Laguerre–Gaussian mode can be rewritten as the superposition of spiral harmonics

$$u'(\rho,\varphi) = u_{00}^{\mathrm{LG}}(\rho,\varphi)\sum_{m=-\infty}^{+\infty} J_m(\alpha\rho) \times \exp\left[\mathrm{i}m\left(\varphi-\delta+\frac{\pi}{2}\right)\right]. \tag{17}$$

Similar to expression (10), the modes decomposition reads

$$u_{\mathrm{f}}(\rho',\varphi') = 2\pi\sum_{n=-\infty}^{+\infty} A_n \sum_{m=-\infty}^{+\infty}\exp\left[-\mathrm{i}m\left(\delta-\frac{\pi}{2}\right)\right] \times \sum_{p=0}^{+\infty} c_{pm}\mathrm{i}^{2p+|m+nl|} u_{p,m+nl}^{\mathrm{LG}}(\rho',\varphi') \otimes\left[\delta\left(\omega_x - nk\sin\theta\right)\delta\left(\omega_y\right)\right], \tag{18}$$

where

$$c_{pm} = \int_0^{+\infty}\int_0^{2\pi} u_{00}^{\mathrm{LG}}(\rho,\varphi)\,J_m(\alpha\rho) \times \exp\left(\mathrm{i}\left(m+nl\right)\varphi\right) u_{p,m+nl}^{\mathrm{LG}^*}(\rho,\varphi)\,\rho\mathrm{d}\rho\mathrm{d}\varphi. \tag{19}$$

3.3. Elliptical profile of incident beams

In many cases the incident beam is not a perfectly symmetric beam, but it has an elliptical beam profile. As shown in Fig.2(c), the incident beam is co-axial with the optical system and has an elliptical profile with a long radius w_{a}, short radius w_{b} and long axis rotation γ.

We consider an elliptical fundamental Gaussian beam with the following form:

$$u'(\rho,\varphi) = \sqrt{\frac{2}{\pi}}\frac{1}{\sqrt{w_{\mathrm{a}}w_{\mathrm{b}}}}\exp\left[-\rho^2\left(\frac{\cos^2(\varphi-\gamma)}{w_{\mathrm{a}}^2}+\frac{\sin^2(\varphi-\gamma)}{w_{\mathrm{b}}^2}\right)\right]. \tag{20}$$

Similar to expression (13), we can obtain

$$u'(\rho,\varphi) = \sqrt{\frac{2}{\pi}}\frac{1}{\sqrt{w_{\mathrm{a}}w_{\mathrm{b}}}}\exp\left(-\frac{\rho^2}{2w_{\mathrm{a}}^2}+\frac{\rho^2}{2w_{\mathrm{b}}^2}\right)\sum_{m=-\infty}^{+\infty} I_m\left(-\frac{\rho^2}{2w_{\mathrm{a}^2}}+\frac{\rho^2}{2w_{\mathrm{b}}^2}\right)\exp\left[\mathrm{i}m\left(2\varphi-2\gamma\right)\right]. \tag{21}$$

By using a similar method in paragraphs 3.1 and 3.2, the mode decomposition reads

$$u_{\mathrm{f}}(\rho',\varphi') = 2\pi\sum_{n=-\infty}^{+\infty} A_n \sum_{m=-\infty}^{+\infty}\exp\left(-\mathrm{i}2m\gamma\right)\sum_{p=0}^{+\infty} c_{pm}\mathrm{i}^{2p+|2m+nl|} u_{p,2m+nl}^{\mathrm{LG}}(\rho',\varphi') \otimes\left[\delta\left(\omega_x - nk\sin\theta\right)\delta\left(\omega_y\right)\right], \tag{22}$$

where

$$c_{pm} = \int_0^{+\infty}\int_0^{2\pi}\sqrt{\frac{2}{\pi}}\frac{1}{\sqrt{w_{\mathrm{a}}w_{\mathrm{b}}}}\exp\left(-\frac{\rho^2}{2w_{\mathrm{a}}^2}-\frac{\rho^2}{2w_{\mathrm{b}}^2}\right) I_m\left(-\frac{\rho^2}{2w_{\mathrm{a}}^2}+\frac{\rho^2}{2w_{\mathrm{b}}^2}\right) \times \exp\left(\mathrm{i}\left(2m+nl\right)\varphi\right) u_{p,2m+nl}^{\mathrm{LG}^*}(\rho,\varphi)\,\rho\mathrm{d}\rho\mathrm{d}\varphi. \tag{23}$$

After the analysis, we can conclude that the nonideal incident beams will lead to an aberrance of the ideal pattern in the far field. Generally speaking, in the nonideal case the spiral spectra[29] are distorted.

4. Discussion

4.1. Perfect conditions

Figure 3 shows the weights of decomposition of the first order diffractive bean, relative powers of orbital angular momentum eigen-states, and the far field diffractive pattern of a field generated with a one-fork binary amplitude grating displaced in Fig.1(b) in perfect collimation. This process is of a common method to generate a Laguerre–Gaussian beam. As shown in Fig.3(a), the weight of Laguerre–Gaussian beam with radial numbers, 0 and +1, is about 78.54%. It means that the generated Laguerre–Gaussian beam is not a pure one. As shown in Fig.3(b), the relative power of orbital angular momentum eigen-states with an azimuthal number of +1 is not 1.0, which is not in agreement with the theoretical prediction in Section 2, because in the numerical simulation the limited radial numbers (less than 5) and the azimuthal numbers (bigger than –3 and less than +5) conduce to the leakage of some states. The relative power is the so-called spiral spectrum[29] or orbital angular momentum spectrum[30] which represents the energy weight for each one of orbital angular momentum eigen-states and can be obtained by adding up all the weights of Laguerre–Gaussian beams with the same azimuthal numbers. It is clear that in the ideal case the gratings can generate rather pure orbital angular momentum eigen-states but not pure Laguerre–Gaussian beam.

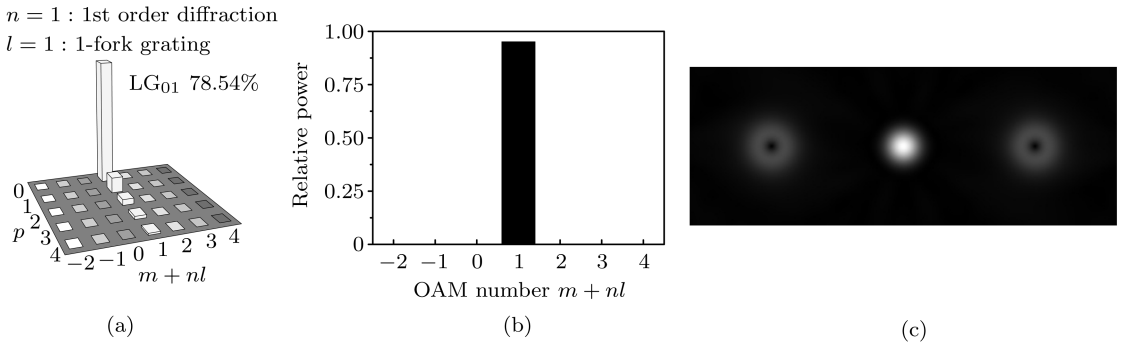


Fig.3. Mode decompositions of the first order diffractive beam (a), relative powers of orbital angular momentum eigen-states (b), and far field diffractive pattern of diffraction of one-fork binary amplitude grating in a perfect condition (c).

4.2. Lateral displacement

Figure 4 shows the weights of mode decompositions of Laguerre–Gaussian beams, relative powers of orbital angular momentum eigen-states, and the far field diffractive patterns of a field generated with a one-fork binary amplitude grating displayed in Fig.1(b), when there exist lateral displacements of $0.2\,w_0$ (up row) and $1.0\,w_0$ (down row) with respect to the x-axis, i.e. $\gamma = 0$, where w_0 is the waist radius of the incident fundamental Gaussian beam. The decomposition makes clear the degradation of the first order diffractive mode from the ideal LG_{01} mode. In Fig.4(a), the weight is about 76.97% with a $0.2\,w_0$ displacement. And Fig.4(d) shows a weight of 44.11% for a $1.0\,w_0$ displacement. It suggests that a bigger beam radius w_0 appears in generating Laguerre–Gaussian modes, for a bigger radius means a better error-tolerance, with lateral displacement existing. We also notice that the dispersion of the modes about a radial number p is suppressed, but about the azimuthal number $m + nl$ it is aggravated with the lateral displacement increasing. It indicates that the lateral displacement degrades the azimuthal structure of the diffractive beam intensively but affects the radial structure slightly. Figure 4(b) indicates the relative power of the total modes with the same orbital angular momentum quantum numbers, which is named as spiral spectra or orbital angular momentum spectra.[29] The spectrum for an azimuthal number of +1 without any lateral displacement does not equal 1.0 because the series of modes are truncated by the limited $p < 5$ in our simulation. From the spiral spectra the dispersion of the azimuthal numbers is obvious. We can

also obtain that when the displacement is $0.2\,w_0$ the energy is almost concentrated into a quantum state with an azimuthal number of +1 and a weight of about 90% in Fig.4(b). Therefore the diffractive grating is not excellent for generating a pure Laguerre–Gaussian beam but it can be used to detect an orbital angular momentum eigen-state with a certain azimuthal number. But with a bigger displacement the spiral spectrum disperses seriously as shown in Fig.4(e). Figure 4(c) shows the simulation diffractive patterns with a $0.2\,w_0$ lateral displacement. The simulation patterns are shown by the black spots in the spot shifts towards the perpendicular direction when the lateral displacement shifts along the x-direction. When the lateral displacement is $0.2\,w_0$, the circle is not full any more. From expression (14) we can consider the pattern as the superposition of a series of LG modes with different phases and amplitudes. In Fig.4(a) the weights of LG_{00}, LG_{10}, and LG_{02} are not negligible and they conduce to the deflection of the perfect circle together. Figure 4(f) shows a greater shift of the black spot when a bigger displacement takes place.

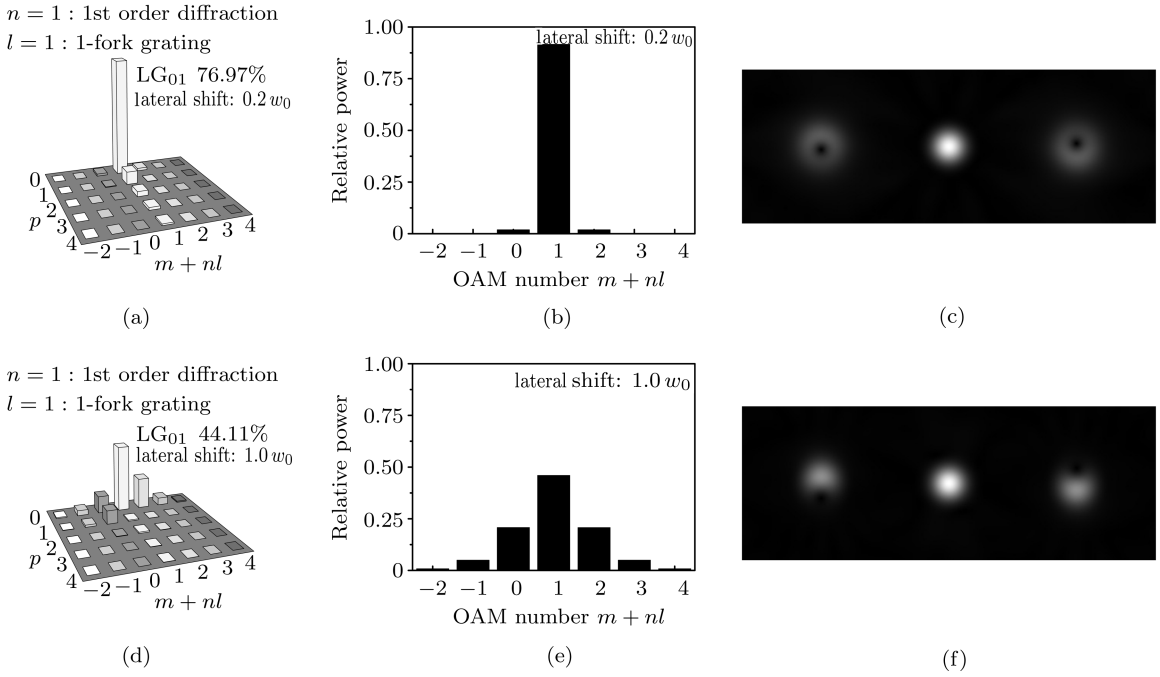


Fig.4. Mode decompositions of the first order diffractive beam (a) and (d), relative powers of orbital angular momentum eigen-states (b) and (e), and far field diffractive patterns of diffraction of one-fork binary amplitude grating with a lateral displacement (c) and (f).

4.3. Angular deflection

Figure 5 shows the results of diffraction of angular deflection with a deflection angle (δ) of 0. The deflection angle is scaled with the first order diffractive angle λ/Λ of the grating, where Λ is the raster constant. We can clearly see from Fig.5(a) that the incident angle is so rigorous that even a $0.05\lambda/\Lambda$ deflection will induce a rather great change of LG_{01} mode. But the results of modes decomposition are different from those for the lateral displacement. The weights of the modes disperse to the modes with bigger radial numbers when the azimuthal number is +1 and to those with adjacent azimuthal numbers when the radial number is 0. While with such a difference, the spiral spectra are dispersed as shown in the ideal case (see Fig.5.(b)). Then we can conclude that a not so rigorous condition can be fulfilled when the raster constant is rather small. Figure 5(c) shows that the diffractive patterns are perfect except for a displacement along the direction of x-axis, which is different from those in the case of lateral displacement where the diffractive pattern is distorted. An easy resolution of side shifting the detector can be taken to obtain the near ideal diffractive pattern. Figures 5(d), 5(e) and 5(f) show similar results to those from Figs.5(a), 5(b) and 5(c) with an angular deflection of $0.2\lambda/\Lambda$. With bigger angular deflections, heavier mode dispersion and spiral spectrum dispersion occur, and side-shifts of diffractive patterns are greater.

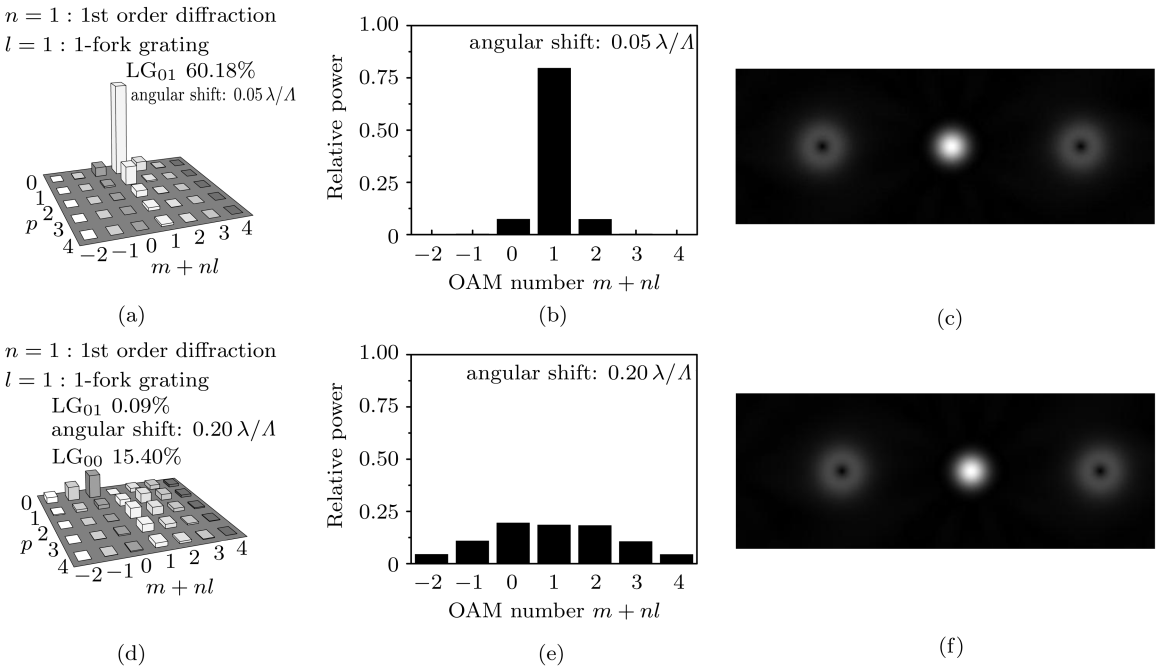


Fig.5. Mode decompositions of the first order diffractive beam (a) and (d), relative powers of orbital angular momentum eigen-states (b) and (e), and far field diffractive pattern of diffraction of one-fork binary amplitude grating with angular deflection (c) and (f).

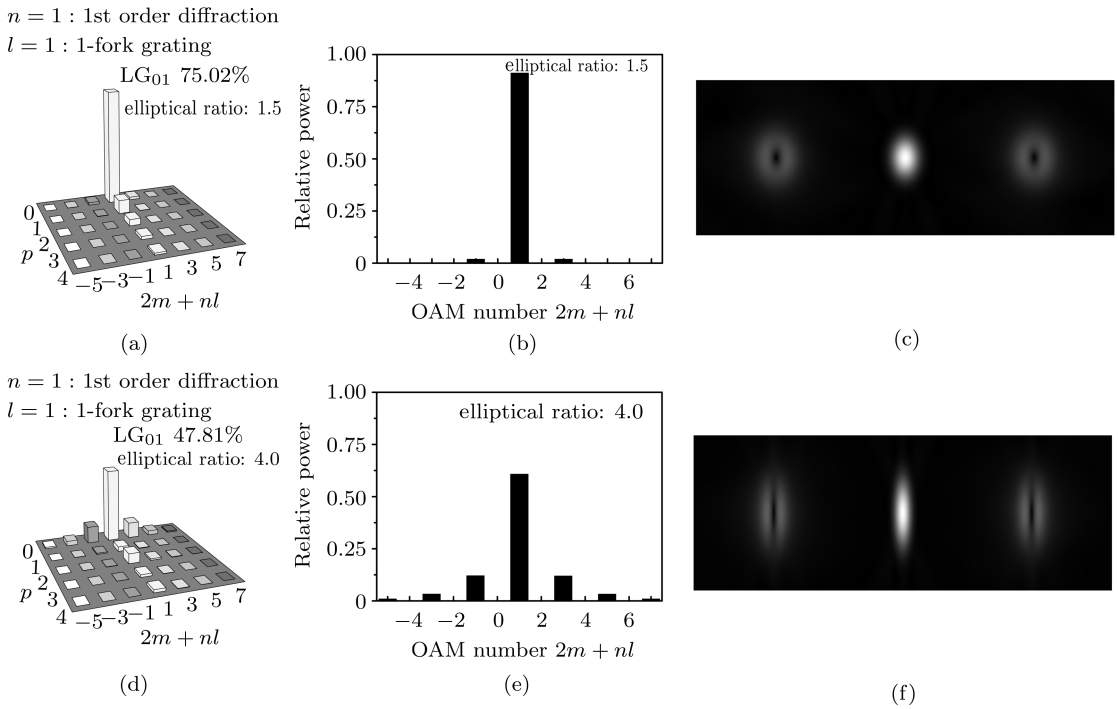


Fig.6. Mode decompositions of the first order diffractive beam (a) and (d), relative powers of orbital angular momentum eigen-states (b) and (e), and far field diffractive pattern of diffraction of one-fork binary amplitude grating illuminated by elliptical incident fundamental Gaussian beam (c) and (f).

4.4. Elliptical incident

Figure 6 shows the results of elliptical incident beams with $\gamma = 0$ and $w_a/w_b > 1$. It is some different from Fig.5 that the azimuthal numbers disperse by two but not one as shown in Fig.6(b). In Fig.6(a), the elliptical incident profile does not affect the radial structure seriously even when w_a/w_b is 1.5. We can conclude that the elliptical incident profiles do not destroy the mode weight distribution intensively. In Fig.6(c), although the mode weight distribution is slight, the diffractive patterns change greatly because the elliptical incident profiles can afford to have different modes with different phase delays as shown in expression (22) and Fig.6(c). The diffractive patterns change from a circle with the same intensity to two quasi-parallel fringes along the short axis direction. Figures 6(d), 6(e) and 6(f) show similar results with a w_a/w_b of 4.0. It is interesting that even when w_a/w_b is 4.0 the orbital angular momentum eigen-state is also distinct.

Although in different conditions, the total orbital angular momentum of diffractive beams does not change. Here, we take into account only the separate influences of these non-ideal cases, but it must be more complex in a mixed case. Because of the potential applications in dada transmission and the easy distortion in transmission, a much more evident and easy correction method is in investigation.

5. Conclusions

In this paper, we discuss the far-field diffractive pattern, mode decomposition and spiral spectrum characteristics in some non-ideal cases of the incident beam when it is used for generating the Laguerre–Gaussian mode or detecting orbital angular momentum eigen-states. In our work, the theoretical results and numerical analyses are both applied to the analysis of the effects in these non-ideal cases.

References

[1] Allen L, Beijerbergen M W, Spreeuw R J C and Woerdman J P 1992 *Phys. Rev.* A **45** 8185

[2] Amos B and Gill P 1995 *Meas. Sci. Technol.* **6** 248

[3] Gao M, Gao C, He X, Li J and Wei G 2004 *Acta Phys. Sin.* **53** 413 (in Chinese)

[4] He H, Friese M E J, Heckenberg N R and Rubinsztein-Dunlop H 1995 *Phys. Rev. Lett.* **75** 826

[5] Dholakia K, Spalding G and MacDonald M 2002 *Phys. World* **15** 31

[6] Molloy J E and Padgett M J 2002 *Contemp. Phys.* **43** 241

[7] Harwit M 2003 *Astrophys. J.* **597** 1266

[8] Voogd R J, Singh M and Braat J J M 2004 *Proc. SPIE* **5380** 387

[9] Liu Y D, Gao C, Gao M and Li F 2007 *Acta Phys. Sin.* **56** 854 (in Chinese)

[10] Gibson G, Courtial J, Vasnetsov M, Barnett S and Franke-Arnold S 2004 *Proc. SPIE* **5550** 367

[11] Zou X and Mathis W 2005 *Phys. Rev.* A **71** 042324

[12] Nihira H and Stroud C R Jr 2005 *Phys. Rev.* A **72** 022337

[13] Torner L, Torres J P and Carrasco S 2005 *Opt. Exp.* **13** 873

[14] Tam C 1988 *Phys. Rev.* A **38** 5960

[15] Beijersbergen M W, Allen L, van der Veen H E L O and Woerdman J P 1993 *Opt. Commun.* **96** 123

[16] Padgett M, Arlt J, Simpson N and Allen L 1996 *Am. J. Phys.* **64** 77

[17] Khonina S N, Kotlyar V V, Shinkaryev M V, Soifer V A and Uspleniev G V 1992 *J. Mod. Opt.* **39** 1147

[18] Ishaaya A A, Machavariani G, Davidson N, Friesem A A and Hasman E 2003 *Opt. Lett.* **28** 504

[19] Bazhenov V Y, Vasnetsov M V and Soskin M S 1990 *JETP Lett.* **52** 429

[20] Heckenberg N R, McDuff R, Smith C P and White A G 1992 *Opt. Lett.* **17** 221

[21] He H, Heckenberg N R and Rubinsztein-Dunlop H 1995 *J. Mod. Opt.* **42** 217

[22] Leach J, Padgett M J, Barnett S M, Franke-Arnold S and Courtial J 2002 *Phys. Rev. Lett.* **88** 257901

[23] Leach J, Courtial J, Skeldon K and Barnett S M 2004 *Phys. Rev. Lett.* **92** 013601

[24] Vasnetsov M V, Pas'ko V A and Soskin M S 2005 *New J. Phys.* **7** 46

[25] Li F, Gao C, Liu Y D and Gao M 2008 *Acta Phys. Sin.* **57** 860 (in Chinese)

[26] Bogush A J Jr and Elkins R E 1986 *IEEE Trans. Antennas Propag.* **AP-34** 228

[27] Abramowitz M and Stegun I (ed) 1964 *Handbook of Mathematical Functions* (Washington, DC: National Bureau of Standards)

[28] Gori F and Guattari G 1987 *Opt. Commun.* **64** 491

[29] Torner L, Torres J P and Carrasco S 2005 *Opt. Exp.* **13** 873

[30] Molina-Terriza G, Torres J P and Torner L 2002 *Phys. Rev. Lett.* **88** 013601